A laser-induced dual ultrasonic wave method for noncontact load monitoring of pillar porcelain insulators

OPEN ACCESS
IOP Publishing
Measurement Science and Technology
Meas. Sci. Technol. **34** (2023) 035205 (10pp)
https://doi.org/10.1088/1361-6501/acaa4d

A laser-induced dual ultrasonic wave method for noncontact load monitoring of pillar porcelain insulators

Zhou-Feng Zhao[1,2,*], Qian Feng[3], Yang Hui[4], Kuang-Da Lu[2], Xiao-Ying Li[1], Bo Ye[1], Jun Zhang[5,*] and Tao Song[6,*]

[1] Zhejiang Electric Boiler and Pressure Vessel Inspection Institute Co., Ltd, Hangzhou 310014, People's Republic of China
[2] Electric Power Research Institute of State Grid Zhejiang Electric Power Co., Ltd, Hangzhou 310014, People's Republic of China
[3] State Grid Zhejiang Power Supply Company Taizhou Branch, Taizhou 318050, People's Republic of China
[4] Hangzhou Yineng Electric Power Technology Co. Ltd, Hangzhou 310014, People's Republic of China
[5] School of Power and Mechanical Engineering, Wuhan University, Wuhan 430072, People's Republic of China
[6] College of Machinery and Automation, Zhixing College of Hubei University, Wuhan, Hubei 430011, People's Republic of China

E-mail: 358576048@qq.com, zhangjun2010@whu.edu.cn and songtao185880@163.com

Received 10 September 2022, revised 27 November 2022
Accepted for publication 9 December 2022
Published 21 December 2022

Abstract

In this paper, a noncontact load monitoring method based on laser-induced synchronous ultrasonic surface wave and air wave is presented to improve the accuracy of load measurement on pillar porcelain insulator. In order to eliminate the measurement error caused by insulator deformation, a correction algorithm for surface wave velocity calculation is established by introducing the air wave propagation time. An experimental setup of the load measurement system for pillar porcelain insulators based on laser-induced dual ultrasonic waves was assembled. A load calibration experiment and load detection experiment were carried out under various bending and torsional loads. The results showed that the proposed method is effective to solve the problem of the surface wave propagation time changing abruptly, greatly increasing the accuracy of load measurement. In the monitoring experiments, the relative error between the calculated load value and the actual applied load value was small, the average measurement error of the bending load was 16.20%, and the average measurement error of the torsional load was 11.38%. This proved that the measurement of the insulator load value using a laser ultrasonic surface wave is more precise than the traditional methods, making it more suitable for engineering inspection.

* Authors to whom any correspondence should be addressed.

Keywords: laser ultrasonic wave, pillar porcelain insulators, load monitoring, surface wave, air wave

(Some figures may appear in colour only in the online journal)

1. Introduction

Pillar porcelain insulators are important components in power plants and substations that support and insulate transmission lines and ensure the normal operation of the pillar porcelain insulator, which is of great significance to the safety of power equipment [1, 2]. Pillar porcelain insulators are prone to large stress concentrations due to installation errors, harsh environments, improper operation, and other factors during application [3, 4]. Moreover, cracks, pores, and other defects will inevitably occur in the production process [5, 6]. Local stress concentration will lead to the continuous expansion of the defects and sudden fracture of the brittle insulator [7]. The fracture of the pillar porcelain insulator often causes serious safety accidents. According to the statistics, 85% of substation safety accidents are caused by the fracture of the pillar porcelain insulator. In order to reduce the occurrence of insulator fracture accidents, it is necessary to monitor the stress state of the insulator in the service state [8, 9].

Ultrasound has been widely used for stress measurement based on the theory of acoustoelastic effect [10–14]. However, the conventional contact ultrasonic method is not suitable for the in-service monitoring of pillar porcelain insulators, due to the high voltage induced damage to the electrical instrument. The laser ultrasonic testing method is a potential method for the load monitoring with the advantage of noncontact and remote stimulation and picking ultrasound [15–20]. Laser ultrasonic testing allows rapid scanning of the metal material to obtain the residual stress distribution on the two-dimensional plane. Ye *et al* [20] used the surface wave coupled with laser-electromagnetic ultrasonic technology to study the surface/subsurface longitudinal residual stress distribution generated by gas metal arc welding. Duquennoy *et al* [6] used laser ultrasound to study the residual stress of Q235 bars, the results showed that the residual stress value has a strong influence on the surface wave velocity. Zhan *et al* [21] used laser ultrasound to detect the lateral and longitudinal residual stress of the additively manufactured TC4 titanium alloy. According to the papers mentioned above, the ultrasound velocity and the load exhibit negative correlation. However, the relationship between ultrasound velocity and the load in ceramic insulators has not been studied.

The accurate measurement ultrasound velocity is essential condition for load measurement. As for specimens with plain surface, the slope of linear fitting curve of travel time and travel distance is used to represent the velocity of surface wave [21]. However, the insulators in this paper have a curved surface. In addition, the insulators will bend as suffered wind load in working environment. So, the conventional fitting method is hard to control the travel distance in remoted condition, and will introduce errors into the measurement and calculation of the surface wave velocity, which will eventually cause stress detection errors. Therefore, a new method needed to be developed to improve detection accuracy.

Aimed at the above problem, this paper proposes an innovative dual ultrasonic wave me method based on synchronous excitation of surface wave and air wave. The air wave is used to corrects the surface wave error caused by the deformation the ceramic material with irregular structure. This is of great significance for improving laser ultrasonic testing technology, and guiding the theoretical research of ultrasonic testing.

2. Method and setup

2.1. Basic theory of the modified laser-induced dual ultrasonic wave method

The ultrasonic waves that are emitted when a laser beam is directed at a material are very dependent on how the laser beam interacts with the particular material. Once generated, these ultrasonic waves propagate through both the material and the surrounding air. When waves propagate through a material, they are called surface waves, and when they propagate in the surrounding air, they are called air waves [21]. In order to accurately measure the spacing between the excitation laser and the receiving laser, and to exclude the change of spot spacing caused by insulator deformation or insulator lower flange fixing bolt deformation during the bending test, a test system based on simultaneously induced surface waves and air waves was used. Figure 1 shows the schematic diagram of the generation and propagation of the surface waves and air waves induced by a laser pulser on the pillar porcelain insulator specimen surface. It can be seen from figure 1 that the air wave and the surface wave were simultaneously excited by a laser beam on the specimen surface, because the air wave propagated through the air and its propagation was not affected by the deformation of the specimen, so the spot spacing calculated by the air wave was not affected by the deformation of the specimen. The algorithm's correction of the laser spot spacing based on air waves, and calculation of the surface wave velocity by using corrected spot spacing and the surface wave propagation time obtained from the test, will greatly improve the accuracy of the surface wave velocity and therefore increase the accuracy of the stress test system.

Figure 2 shows the waveform of the surface waves and air waves on the pillar porcelain insulators induced by the laser pulser. Cross-correlation calculations of surface waves and air waves in coinstantaneous loading were carried out to obtain the parameters t_s (propagation time of surface wave)

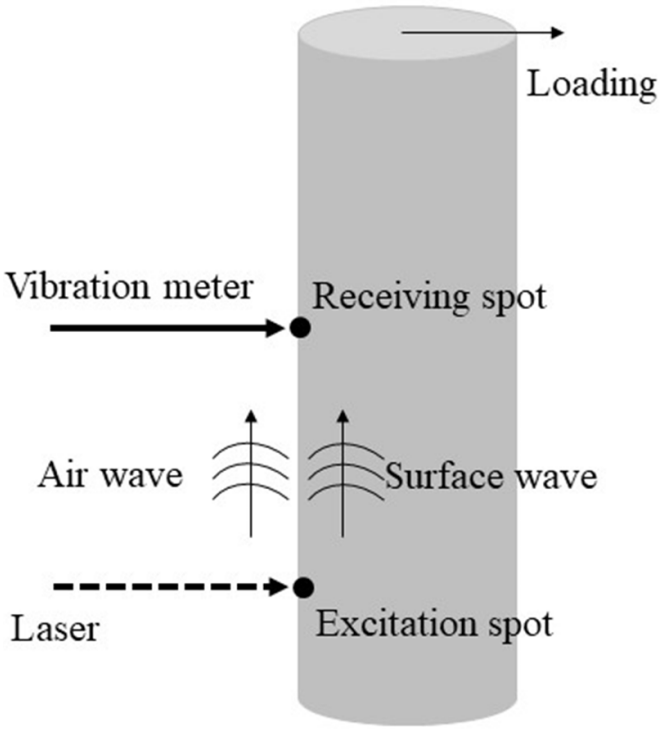

Figure 1. Schematic diagram of the generation and propagation of the surface waves and air waves induced by a laser pulser.

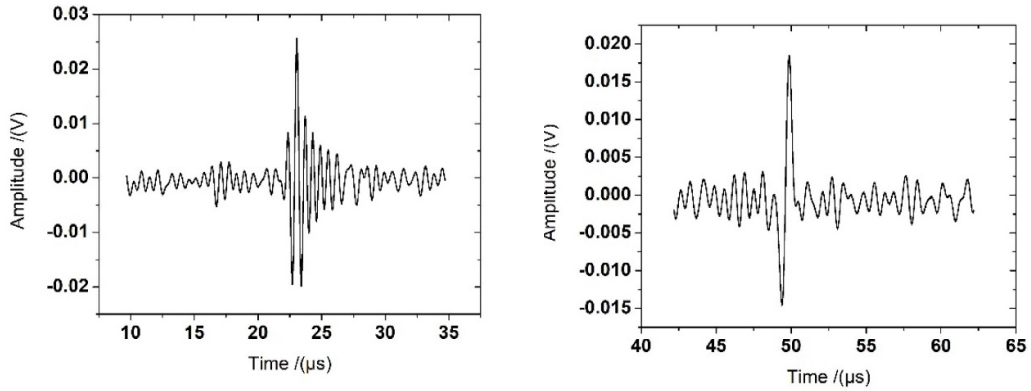

(a) the waveform of the surface wave (b) the waveform of the air wave

Figure 2. The waveform of the surface waves and air waves on the pillar porcelain insulators induced by the laser pulser.

and t_a (propagation time of air wave). The parameter of room temperature T was obtained by the dynamic focusing mirror temperature sensor.

The velocity of air wave v_a can be calculated by the following equation [22]:

$$v_a = 331.4 + 0.607T. \tag{1}$$

Therefore, the distance of the inducing spot and receiving spot d is given by:

$$d = t_a v_a. \tag{2}$$

By obtaining the propagation time of a surface wave, the velocity of the surface waves can be calculated by:

$$v_s = \frac{d}{t_s}. \tag{3}$$

Thus, the velocity of air wave v_s can be obtained at different loads. The velocity changes of the surface wave (Δv) and stress on the pillar porcelain insulator (F_w) satisfy the equation as [23]:

$$\Delta v = kF_w \tag{4}$$

where k is a constant coefficient.

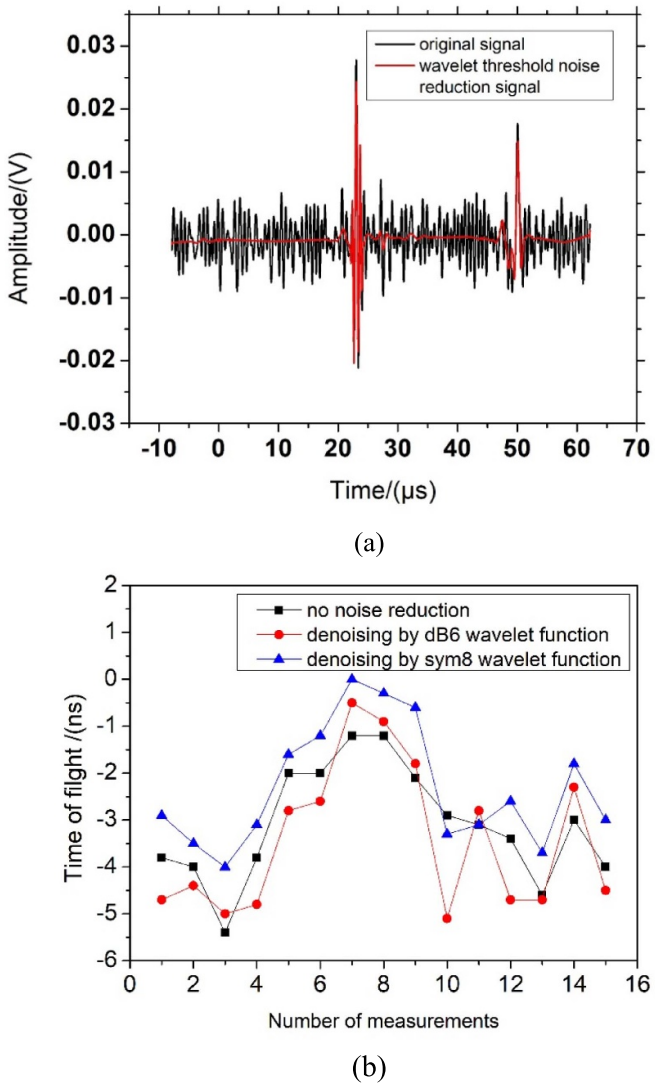

Figure 3. Contrast diagram of ultrasonic signals, (a) is the original signal and wavelet threshold denoising signal, (b) is ultrasonic signals flight time of no noise reduction and denoising by dB6 and sym8 wavelet function.

In practice, the distance between the detecting system and pillar porcelain insulator is relatively far. Therefore, the attenuation of the excitation laser is relatively serious, and will lead to the surface waves and air waves induced by the laser drowning in the noise. Therefore, the wavelet threshold denoising method was adopted to process the signals. In this paper, the wavelet threshold denoising method used the sym8 wavelet as the wavelet base, because the sym8 wavelet function has tight support and good continuity and symmetry, making it suitable for denoising signals with good continuity. Ultrasonic surface wave and air wave signals before and after denoising are shown in figure 3. It can be seen from figure 3(a) that the wavelet threshold denoising algorithm does not change the phase of surface waves and air waves and has an excellent denoising effect, which is convenient for subsequent signal processing. Figure 3(b) show that the noise reduction effect of sym8 wavelet function is much better than the dB6 wavelet function.

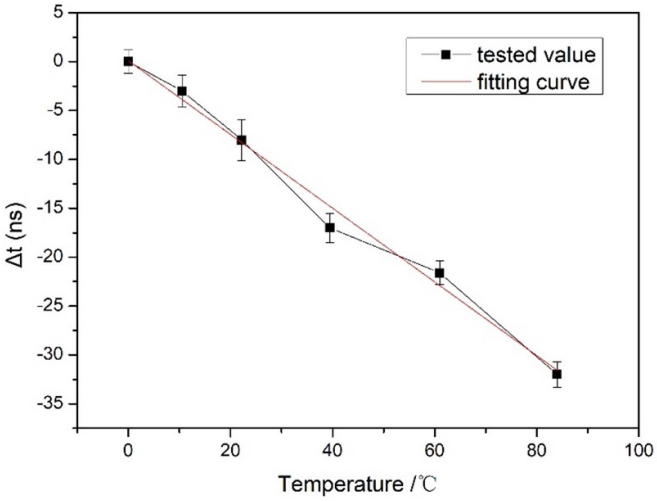

Figure 4. The linear relationship between the temperature of the pillar porcelain insulators and the time of flight of the ultrasonic wave.

In order to accurately extract the variation of the propagation time of the surface waves and air waves, and to reduce the testing error of the propagation time caused by the change of waveform amplitude, a cross-correlation calculation of the interpolated ultrasonic signal was carried out to obtain the variation of the ultrasonic propagation time under various loads. The ultrasonic signal was intercepted and the surface wave signal was cross-correlated separately, which reduced the influence of the similarity of the noise signal and other clutter signals on the phase difference of the surface wave signal.

Temperature is significant to the ultrasonic velocity. The time of flight of ultrasound propagate in the insulators under different temperature were measured and shown in figure 4. It shows that the time of flight decreases with the increase of temperature. The figure also depicts the fitting curve. There is a very good linear relationship, with the fitting curve equation being $y = -0.377x + 0.098$. The fitting curve in figure 4 can be used to correct the time of flight and velocity of an ultrasonic wave. However, the following tests in this paper were conducted at a specific temperature, in order to focus on the discussion of load measurement based on synchronous excitation of surface wave and air wave.

2.2. Experimental setup

The experimental setup of the stress detection system for the pillar porcelain insulators based on laser-induced dual ultrasonic waves is shown in figure 5. The laser model used by the laser ultrasonic emission module was EO-1064-N. The laser center wavelength emitted by this laser is 1063.551 nm. When the pulse frequency of the laser was 1 KHz, the average power was 882.7 mW, the output energy of the optical outlet was 0.92 mJ, and the laser divergence angle was about 2 mrad. The pulse width of the pulsed laser was 6.881 ns. To protect the glaze layer on the insulator surface, a dynamic focusing mirror was used to adjust the laser focusing state.

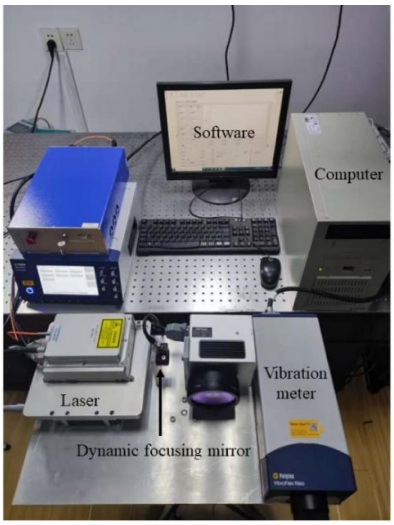

(a)

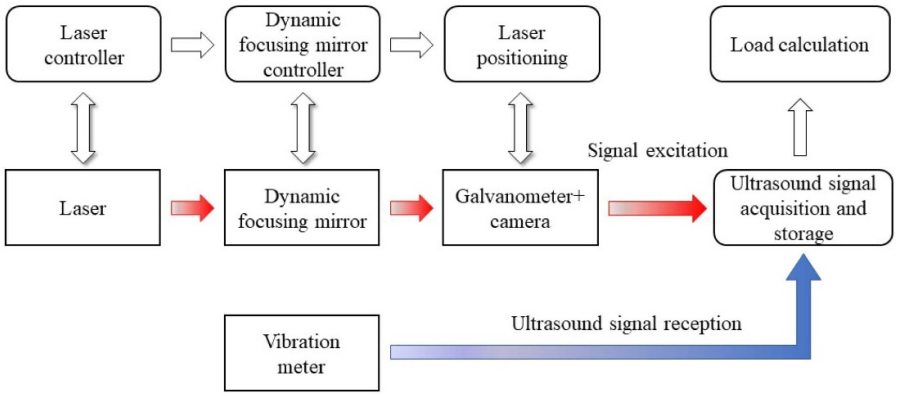

(b)

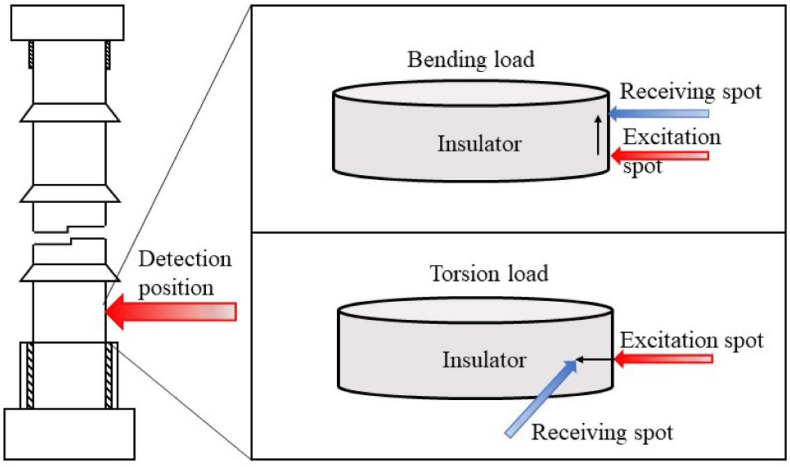

(c)

Figure 5. Experimental setup of the stress detection system for the pillar porcelain insulators based on laser-induced dual ultrasonic waves: (a) physical map of the detection system, (b) working principal diagram, (c) schematic of the specimens in the experiment.

The dynamic focusing mirror was EL-10-30-Ci, from the Optotune company. The focal length of the dynamic focusing mirror could be adjusted within the range of −1.5 to 3.5 dpt. The upper computer controlled the current to adjust the focal length. The maximum input current of the dynamic focusing mirror was 300 mA. In order to ensure the relative position

Figure 6. Photographs of the pillar porcelain insulator load detection system based on laser ultrasound.

of the excitation laser spot and the receiving laser spot, the excitation laser was deflected with a polarizer. The type of polarizer used in the system was a SCANcube-10, and the repeated positioning accuracy of the galvanometer was less than 2 μrad, satisfying the requirements of laser spot position adjustment. The polarizer was controlled by a SCANLAB RTC5 card. The laser ultrasonic receiving module used a Poly-Tec's high-performance single-point laser Vibroflex, which has a laser wavelength of 633 nm and a frequency range of 0–24 mhz. The receiving module received ultrasonic signals from the NI PCI-5153 data acquisition board produced by National Instrument. The sampling frequency of the board was 2 GHz, and the sampling length was 50 000 sampling points.

2.3. Experimental scheme

In order to verify the load measurement method for pillar porcelain insulators based on the laser-induced dual ultrasonic wave method, calibration and testing experiments were carried out on the pillar porcelain insulators in bending and torsion experiments. The bending and torsion tester model was QH-WQ-100 K, the rated bending force was 100 KN, and the rated torsion force was 20 KN m, as shown in figure 6. In the bending test, the pillar porcelain insulators were fixed by anchor bolts, and transverse bending loads of 1 KN, 2 KN, 3 KN, 4 KN, and 5 KN were applied to the upper flange. In the torsion experiment, the upper end of the pillar porcelain insulator was fixed, and the lower end was rotated clockwise. Torsion loads of 0.7 KN m, 1.4 KN m, 2.1 KN m, 2.8 KN m, and 3.5 KN m were applied. The location of laser ultrasonic detection was between the lower flange of the insulator and the first umbrella skirt, 30–50 mm away from the lower flange, as shown in figure 5(c). Since the stress directions on the surface of the insulator under the action of bending load and torsional load were different, the direction of the principal stress on the surface of the insulator under the action of the bending load was parallel to the normal line of the insulator ceramic column, while the direction of the principal stress on the surface of the insulator under the action of the torsion load was along the axial direction of the insulator surface. To ensure that the surface wave propagation direction was parallel to the principal stress direction on the surface of the insulator, the excitation and receiving laser spots were arranged vertically in the bending test, while the two spots were distributed horizontally along the axial direction in the torsion experiment.

3. Experiment results and discussion

3.1. Analysis of bending load calibration experiment results of pillar porcelain insulators

Figure 7(a) shows the surface wave propagates time-load diagram in the bending tensile stress region, where the abscissa represents the transverse bending load loaded on the porcelain insulator, and the ordinate represents the surface wave propagate time. It can be seen that when the load is 2 KN and 3 KN, the propagation time of the surface wave changes abruptly, and the propagation time of the surface wave before and after the sudden change shows a good linear relationship with the load value. The reason for this is the deformation of the porcelain insulator and the deformation of the anchor bolt during the loading process. The detection position has a large

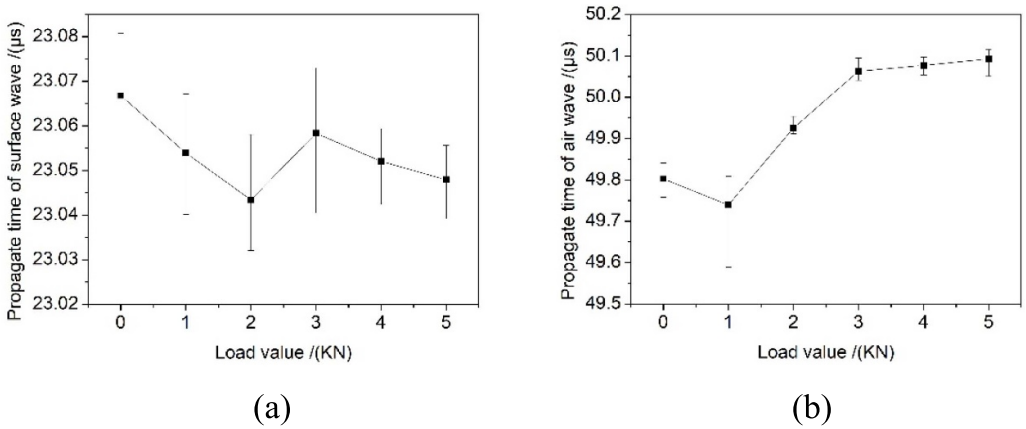

Figure 7. Propagation time of the surface waves and air waves under various loads: (a) surface wave and (b) air wave.

Table 1. Changes of surface wave propagation time, air wave propagation time, and spot spacing with loading after correction.

Load value/(KN)	0	1	2	3	4	5
Surface wave propagate time /(μs)	3.0668	3.0539	3.0564	3.0583	3.0520	3.0479
Air wave propagate time /(μs)	29.8026	29.7393	29.9257	30.0629	30.0768	30.0925
Spot spacing /(μm)	10 044.8	10 023.4	10 086.2	10 132.5	10 137.1	10 142.4

displacement, and there are different degrees of eccentricity during the installation of the pillar porcelain insulator. During the lateral bending stress loading, the deformation of each part is uneven, resulting in the change in the distance between the excitation laser and the receiving laser spot. Figure 7(b) shows the air wave propagate time-load diagram in the bending tensile stress region. It can be seen from figure 7(b) that when the load is less than 3 KN, the propagation time of the air wave gradually decreases, and the distance between the laser spots gradually decreases. When the load is 3 KN, the propagation time of the air wave changes abruptly, which is consistent with the changing trend of the propagation time of the surface wave. After 3 KN, the air wave propagation time changes less. The spot spacing varies less.

The system read that the temperature of the experimental site was 9.3 °C, and the air temperature was brought into the calculation formula of the air wave sound speed equation (1), from which we obtained the air wave speed of 337.04 m s^{-1} during the experiment. The vibrometer used in this system had a system delay of 20 μs when the bandwidth frequency was 1 MHZ, so the propagation time of the surface waves and air waves obtained was subtracted from the system delay.

Table 1 shows the surface wave propagation time t_s and the air wave propagation time t_a after subtracting the system delay. The spot spacing under each load was calculated by the air wave propagation time and the air wave speed according to equation (2). Finally, the surface wave velocity V_s under each load was obtained by equation (3).

After synchronous excitation, the air wave–surface wave was modified, and the surface wave velocity–load curve shown in figure 8 was obtained. The surface wave velocity increased from 3275.31 m s^{-1}–3327.63 m s^{-1}. Under a load of 5 KN, the wave velocity change was 52.32 m s^{-1} compared with a load of 0 KN. Using the obtained surface wave velocity–load curve, the surface wave velocity change rate-load curve was obtained, as shown in figure 8(b). The fitting equation of this curve is $y = 11.21315x - 0.08208$, and in the load calibration equation, the calibration coefficient $K = 11.213\,15$. The linear regression coefficient of determination $R2 = 0.968\,56$, with good linearity.

After the insulator bending load calibration curve was obtained, the insulator bending load value could be calculated using the calibration curve. First, the system was used to collect the propagation time of the surface waves and air waves of the insulator, to calculate the surface wave velocity, and then to calculate the surface wave velocity change rate. The calculated load value could be obtained by substituting the wave velocity change rate into the load calibration equation obtained in the previous section.

Figure 9 shows the comparison curve between the calculated load value and the actual load value. We calculated its relative error and absolute error, as shown in figure 9(b). As can be seen from the figure, when the load was 3 KN, the absolute error was the largest at 0.96 KN, and when the load was 2 KN, the absolute error was the smallest at 0.10 KN. The relative error was the largest at 32.03%, and the smallest was 5.21%. Taking the average value of the relative error, the average error of the bending load detection was 16.20%.

In the process of using the laser ultrasonic surface wave to detect the bending load of the insulator, the error sources included: a. During the firing process of the insulator, the viscosity of the glaze is relatively high, and it cannot fully cover the insulator ceramic embryo, which will cause uneven glazing of the insulator and affect the propagation of surface waves. b During the actual collection process, due to the insulator's deformation, the vibrometer laser will be out of focus,

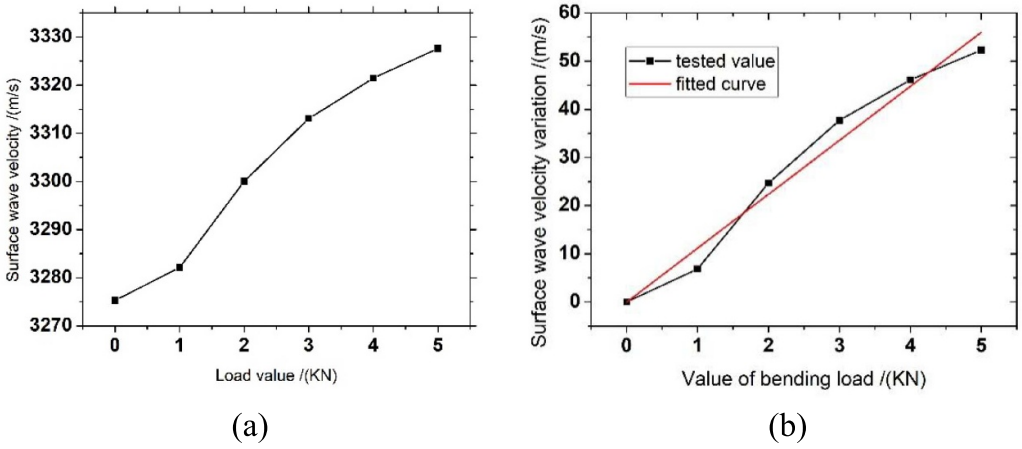

Figure 8. Results of the modified surface wave velocity, surface wave velocity variation, and linear fitting curve under various loads: (a) modified surface wave velocity, (b) surface wave velocity variation and linear fitting curve.

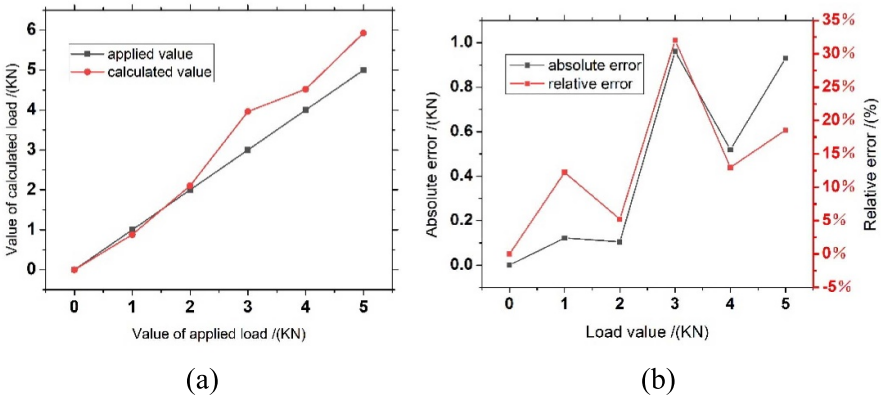

Figure 9. Comparison between the experimental calculated load value and the actual load value and the absolute error and relative error: (a) the calculated load and actual load, (b) the absolute error and relative error.

resulting in a low signal-to-noise ratio and unstable waveform phase under a certain load, which affects the surface wave velocity calculation.

3.2. Analysis of torsional load calibration experiment results of pillar porcelain insulators

Since the distance between the excitation laser on the surface of the insulator and the received laser spot does not change during the torsion process, in this experiment, only the surface wave data was collected, and the torque calibration curve used the following formula:

$$|\Delta t| = KF_{\mathrm{N}} \tag{5}$$

where Δt is the change in the propagation time of the surface wave, which is subtracted from the propagation time of the surface wave under the initial state t_0 to be the propagation time t of the surface wave after the load is applied, F_{N} is the applied torque, and K is the calibration coefficient.

As shown in figure 10, the time-of-propagation of the insulator surface wave changed under various torques. It can be seen from figure 10(a) that with the increase of the applied torque, the torsional shear stress decreases, resulting in the increase of the surface wave propagation time; that is, the surface wave velocity increases with the increase of the torque. Considering that the direction of the torsional shear stress is parallel to the propagation direction of the surface wave at this time, it can be inferred that, when the propagation direction of the surface wave is parallel to the stress direction, as the stress value increases, the surface wave velocity also increases. The conclusions obtained in the tensile stress region were consistent. In figure 10(a), the torque increased from 0.7 KN m to 3.5 KN m, the surface wave propagation time changed from 23.13 μs to 22.90 μs, and the propagation time decreased by 0.23 μs. The fitting curve is shown in figure 10(b); the curve fitting equation is $y = 0.0886x - 0.0697$, and the torque calibration coefficient $K = 0.0886$. The coefficient of determination of linear fitting, $R2 = 0.9738$, indicated that in the torsion experiment, the linearity of the surface wave propagation time and the torque fitting line was better than in the bending experiment.

Using the experimental method, under the condition of constant spot spacing, a torsion experiment was performed on the insulator, and the calculated torque was compared with the actual applied torque to verify the correctness of the torsion

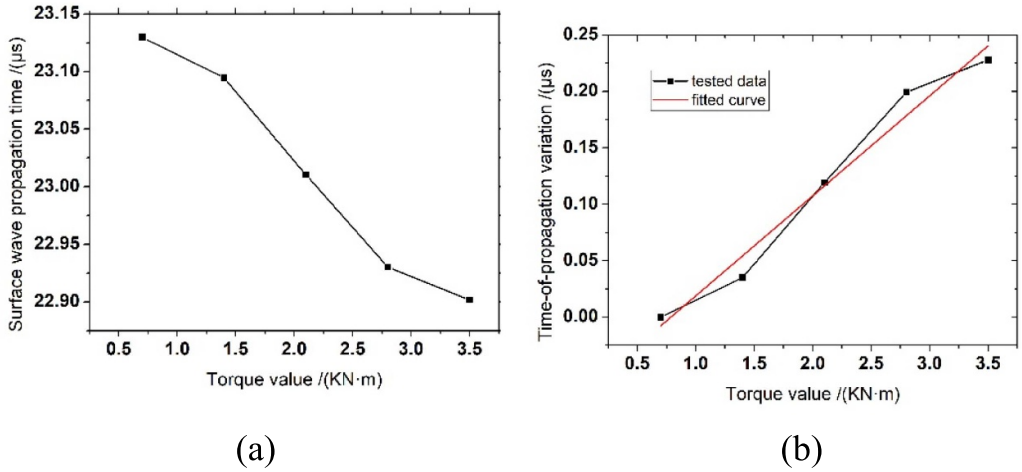

Figure 10. Surface wave propagation time, surface wave time-of-propagation variation, and linear fitting curve under various torques: (a) surface wave propagation time, (b) surface wave propagation time variation and linear fitting curve.

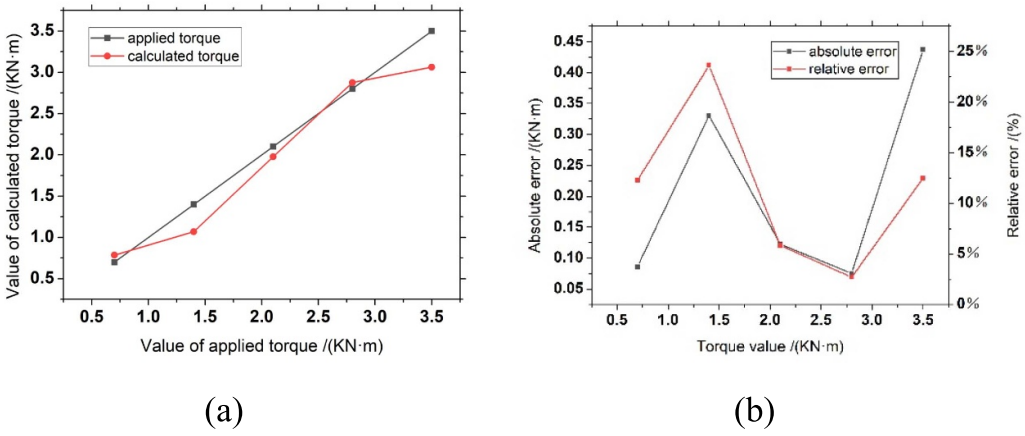

Figure 11. The comparison between the experimental calculated load value and the real load value, the absolute error and relative error: (a) calculated torque vs. applied torque diagram, (b) the relative error and absolute error of the calculated torque.

calibration curve and, at the same time, prove that the system can be used for the detection of torsional stress in insulators.

The time-of-propagation rate of change was brought into the torque calibration curve to obtain the calculated torque value. We compared the calculated torque value with the actual torque value, as shown in figure 11(a). It can be seen that the calculated torque was relatively close to the real torque, and the relative error and absolute error of the calculated torque were calculated to obtain figure 11(b).

As can be seen from figure 11, the maximum absolute error between the calculated torque and the applied torque was 0.40 KN m, the minimum absolute error was 0.05 KN m, and the maximum relative error was 13.18% when the torque was 2.8 KN m. The minimum relative error was 3.91%, which appeared at the torque of 1.4 KN m. The average error in the calculated torque value was 11.38%. It can be seen that, in the torsional load of the insulator detected by the laser ultrasonic surface wave, the relative error was smaller than the bending load measurement.

4. Conclusion

(a) An air wave–surface wave modified algorithm and ultrasonic signal preprocessing method based on synchronous induced by laser were proposed in this paper, and applied to bending load detection experiments for pillar porcelain insulators. This method was able to effectively solve the problem of the surface wave propagation time changing abruptly due to factors such as installation eccentricity, anchor bolt deformation, etc, which greatly increased the accuracy of load measurement.

(b) Using the laser ultrasonic pillar porcelain insulator load detection system, a load calibration experiment and load detection experiment were carried out on the pillar porcelain insulator under bending and torsional loads, and surface wave and air wave data were collected. The ultrasonic signal was processed by the air wave–surface wave correction algorithm based on synchronous excitation, and the bending and torsional load values of the insulator

were calculated and compared with the actual load value. The results showed that the relative error between the calculated load value and the actual load value was small. The average measurement error of the bending load was 16.20%, and the average measurement error of the torsional load was 11.38%, which proves that the detection of the insulator load value using the laser ultrasonic air wave–surface wave method has sufficient accuracy to meet the needs for engineering inspections.

Data availability statement

All data that support the findings of this study are included within the article (and any supplementary files).

Funding

This paper was supported by State Grid Zhejiang Electric Power Co., Ltd Science and Technology Funded Projects (B311DS210014) and Scientific Research Project of Hubei Provincial Department of Education (B2021409).

ORCID iDs

Jun Zhang https://orcid.org/0000-0002-5213-0857
Tao Song https://orcid.org/0000-0002-5151-3493

References

[1] Qiu Z B, Ruan J J, Huang D C, Li X B, Wang F C and Yao W J 2015 Study on glaze electrical erosion characteristics of porcelain post insulator by using inclined plane and graphite-layer-based method *IEEE Trans. Dielectr. Electr. Insul.* **22** 3385–94

[2] Yang L, Shang G F, Kuang Z Q, Sun Y J, Liao Y F, Hao Y P and Li L C 2022 Experimental investigation on flashover characteristics of hollow porcelain insulator under extreme rainfall *Electr. Power Syst. Res.* **203** 8

[3] Wang X, Yu Z Q and He J L 2014 Breakdown process experiments of 110-to 500-kV insulator strings under short tail lightning impulse *IEEE Trans. Power Deliv.* **29** 2394–401

[4] Zhao Y M, Yan J, Wang Y X, Jing Q Z and Liu T L 2021 Porcelain insulator crack location and surface states pattern recognition based on hyperspectral technology *Entropy* **23** 18

[5] Mao H L, Tang W L, Huang Y X, Mao H Y, Huang Z F and Li X X 2020 Research on NOFRF entropy-based detection method for early damage of pillar porcelain insulator *Shock Vib.* **2020** 11

[6] Duquennoy M, Ouaftouh M, Qian M L, Jenot F and Ourak M 2001 Ultrasonic characterization of residual stresses in steel rods using a laser line source and piezoelectric transducers *NDT&E Int.* **34** 355–62

[7] Javadi Y, Akhlaghi M and Najafabadi M A 2013 Using finite element and ultrasonic method to evaluate welding longitudinal residual stress through the thickness in austenitic stainless steel plates *Mater. Des.* **45** 628–42

[8] Nau A and Scholtes B 2013 Evaluation of the high-speed drilling technique for the incremental hole-drilling method *Exp. Mech.* **53** 531–42

[9] Royer D and Chenu C 2000 Experimental and theoretical waveforms of Rayleigh waves generated by a thermoelastic laser line source *Ultrasonics* **38** 891–5

[10] Yang J, Lee H, Lim H J, Kim N, Yeo H and Sohn H 2013 Development of a fiber-guided laser ultrasonic system resilient to high temperature and gamma radiation for nuclear power plant pipe monitoring *Meas. Sci. Technol.* **24** 8

[11] Zamiri S, Reitinger B, Bauer S and Burgholzer P (eds) 2014 Converging laser generated ultrasonic waves using annular patterns irradiation *3rd Int. Symp. on Laser Ultrasonics and Advanced Sensing 2013 (Yokohama, Jun 25-28)* (Bristol: Iop Publishing Ltd)

[12] Tashakori S, Baghalian A, Unal M, Fekrmandi H, Senyurek V Y, McDaniel D and Tansel I N 2016 Contact and non-contact approaches in load monitoring applications using surface response to excitation method *Measurement* **89** 197–203

[13] Ochiai M, Miura T and Yamamoto S (eds) 2008 Laser-ultrasonic testing and its applications to nuclear reactor internals *34th Annual Review of Progress in Quantitative Nondestructive Evaluation 2007 (Jul 22-27)* (Melville, NY: Amer Inst Physics)

[14] Guo J, Fu H Y, Pan B and Kang R K 2021 Recent progress of residual stress measurement methods: a review *Chin. J. Aeronaut.* **34** 54–78

[15] Liu Z W, Lin B, Liang X H and Du A Y 2021 Inversion of surface damage and residual stress in ground silicon wafers by laser surface acoustic wave technology *Ultrasonics* **113** 9

[16] Wang J J, Xu B Q, Shen Z H, Ni X W and Lu J 2009 Influence of transparent coating thickness on thermoelastic force source and laser-generated ultrasound waves *Appl. Surf. Sci.* **255** 7172–8

[17] Murray T W, Deaton J B and Wagner J W 1996 Experimental evaluation of enhanced generation of ultrasonic waves using an array of laser sources *Ultrasonics* **34** 69–77

[18] Masurkar F, Rostami J and Tse P 2020 Design of an innovative and self-adaptive-smart algorithm to investigate the structural integrity of a rail track using Rayleigh waves emitted and sensed by a fully non-contact laser transduction system *Appl. Acoust.* **166** 15

[19] Strgar S and Mozina J 2002 An optodynamic determination of the depth of laser-drilled holes by the simultaneous detection of ultrasonic waves in the air and in the workpiece *Ultrasonics* **40** 791–5

[20] Ye C, Ume I C, Zhou Y L and Reddy V V B 2019 Inspection of the residual stress on welds using laser ultrasonic supported with finite element analysis *Manuf. Rev.* **6** 10

[21] Zhan Y, Liu C, Zhang J J, Mo G Z and Liu C S 2019 Measurement of residual stress in laser additive manufacturing TC4 titanium alloy with the laser ultrasonic technique *Mater. Sci. Eng.* A **762** 10

[22] Pao Y H, Sachse W and Fukuoka H 1984 Acoustoelasticity and ultrasonic measurements of residual-stresses *Phys. Acoust.* **17** 61–143

[23] Kim H, Chang W Y, Kim T and Jiang X N 2020 Stress-sensing method via laser-generated ultrasound wave using candle soot nanoparticle composite *IEEE Trans. Ultrason. Ferroelectr. Freq. Control* **67** 1867–76